ELSEVIER

Thermochimica Acta 395 (2003) 209–216

thermochimica acta

www.elsevier.com/locate/tca

In situ generation of metal clusters in interlamellar spacing of montmorillonite clay and their thermal behaviour

Omar S. Ahmed[a], Dipak Kumar Dutta[b,*]

[a]*Department of Chemistry, Bahona College, Bahona 785101, Jorhat, Assam, India*
[b]*Material Science Division, Regional Research Laboratory (CSIR), Jorhat 785006, Assam, India*

Received 17 April 2001; received in revised form 18 January 2002; accepted 23 March 2002

Abstract

Intercalated Ni–Ni$(CH_3COO)_2$–montmorillonite (**I**), Ni^0–montmorillonite (**II**), Zn–Zn$(CH_3COO)_2$–montmorillonite (**III**) and Zn^0–montmorillonite (**IV**) composites have been synthesised and their thermal behaviour is studied by TG, DTG and DTA substantiated by XRD and TEM. The endothermic DTA peaks of the composites **I**–**IV** due to dehydration and dehydroxylation, in general, occur at lower temperature compared to those of untreated Na–montmorillonite. The phase change of the clay matrix for the composites **I** and **II** takes place at slightly higher temperature compared to Na–montmorillonite, while for the composites **III** and **IV** it occurs at lower temperature. XRD data show that the basal spacing ($d_{0\,0\,1}$ value 13.7 Å) of the intercalated metal cluster composite **II** is higher than that of the composite **IV** ($d_{0\,0\,1}$ value 12.8 Å) at about 300 °C revealing intercalated metal cluster of size 4.1 and 3.2 Å, respectively. TEM study shows that the particle size of the metals for the composite **II** is in the range of about 0–80 nm while for the composite **IV**, the size range is about 0–30 nm. Therefore, bigger sized metal nanoparticles (>0.41 nm) are not present in the interlamellar spacing of the clay.
© 2002 Elsevier Science B.V. All rights reserved.

Keywords: Intercalation; Basal spacing; Metal–montmorillonite composites; Metal acetate–montmorillonite composites; Metal cluster; Metal nanoparticles

1. Introduction

Metals belong to an important class of active catalyst that are used for a broad range of processes including various transformations of hydrocarbons. Metal catalysts are prepared in the form of metal nanoparticles which are stabilised on the surface of various supports [1]. Metal particles of micron and submicron sizes are formed by reduction of inorganic compounds in liquid polyols [2].

In the last few years attempts have been made to incorporate nanoparticles of metals into layered clay minerals like montmorillonite (hereafter Mont) [3,4]. Metal clusters of 4–5 Å in size are formed and the microporous nature of such zero valent metal intercalated clay nanocomposites are also confirmed [4,5]. Such metal clusters, supported on microporous materials, are expected to behave very differently from bulk metals and may exhibit unique catalytic and adsorption properties, molecular selectivity and polyfunctional activity[5]. Clay supported Pd^0 nanoparticles are found to show excellent catalytic activity for hydrogenation in liquid phase [6–8].

* Corresponding author. Tel.: +91-376-3370-121x529; fax: +91-376-3370-011.
E-mail address: dipakkrdutta@yahoo.com (D.K. Dutta).

0040-6031/02/$ – see front matter © 2002 Elsevier Science B.V. All rights reserved.
PII: S0040-6031(02)00215-0

The present work reports investigation on intercalation of nickel acetate and zinc acetate into Na–Mont and subsequent reduction by polyol method to generate in situ the corresponding metal clusters. Thermal stability of the metal acetate–clay and metal cluster–clay composites have been studied by thermogravimetry (TG), differential thermogravimetry (DTG) and differential thermal analysis (DTA) substantiated by X-ray diffraction (XRD) and transmission electron microscopy (TEM).

2. Experimental

2.1. Materials and methods

Montmorillonite clay collected from Crook County, Wyoming USA (SWy-2) Source Clay Minerals Repository contained silica sand, iron oxide, etc. as impurities, and was purified by the sedimentation method [9] to collect the <2 μm fraction. The oxide composition of the clay determined by weight chemical and flamephotometric methods was SiO_2: 58.12%; Al_2O_3: 18.93%; Fe_2O_3: 4.63%; MgO: 2.52%; CaO: 1.12%; LOI: 13.54% and others (Na_2O, K_2O and TiO_2): 1.14%.

The clay was converted to the homoionic Na-exchanged form Na–Mont by stirring in 2M NaCl solution for about 78 h, which was washed and finally dialysed against distilled water until conductivity of the dialysate approached that of distilled water. The cation exchange capacity (CEC) of the clay was found [10] to be 80 meq./100 g of clay.

2.2. Intercalation/intersalation reaction of metal acetate hydrates $M(CH_3COO)_2{\cdot}xH_2O$ (where $M = Ni, Zn$) with Na–Mont

One gram of clay was dispersed in 100 ml water and 24 meq. solid metal acetate (30 times in excess of clay in terms of CEC) was then added to the dispersion. The mixture was kept under stirring for 24 h. The slurry was filtered, washed and dialysed against distilled water until conductivity of the dialysate approached that of distilled water. The samples were dried at 80 °C for 24 h. Such treatment with excess metal salts over CEC of the clay gives initially an intercalated metal ion exchanged product (M–Mont) followed by intersalation reaction, i.e. adsorption of ion-pair $\{M(CH_3COO)_2\}$ on M–Mont resulting a product M–$M(CH_3COO)_2$–Mont which contain about three times CEC equivalent of metal ion.

2.3. Reduction of intercalated/intersalated clay composites by polyol method

An amount of 0.5 g M–$M(CH_3COO)_2$–Mont was suspended in 50 ml ethylene glycol in a double necked round bottom flask and refluxed at 195 °C for 6 h in nitrogen environment to form a reduced solid product M^0–Mont which was recovered and washed with methanol till free from ethylene glycol and then dried in dessicator over silica gel.

The TG, DTG and DTA measurements were done with the Thermal Analyser (TA instruments, Model STD 2960 simultaneous DTA–TGA) with about 20 mg of sample in a platinum crucible at a heating rate of 10 °C min^{-1} in air atmosphere. The TGA weighing mechanism has a sensitivity of 0.1 μg, while the temperature accuracy of the instrument is ±2% to 1000 °C. For basal spacing determination by XRD, thin layered (oriented) samples were prepared on glass slides by standard technique [11] and were dried at 50, 100, 200, 300, 400, 500 and 600 °C for about 1 h. XRD patterns were taken in the range $2\theta = 2$–60° at a rate of 6°/min (X-ray diffractometer JEOL, JDX-11p 3A, Japan) using Cu Kα radiation. Specimens for TEM were prepared by dispersing powdered samples in iso-propyl alcohol and were placed on copper grids and allowed to dry. Sample grids were examined by TEM using smallest condenser aperture using a JEOL model: JEM 100C X11 (100 kV) electron microscope.

3. Results and discussion

3.1. Thermal studies

The TG–DTG–DTA curves of the composites **I** and **II** are shown in Fig. 1. The TG and DTG curves of composites **I** and **II** show first mass loss of 17.7 and 9.6% up to 130 °C, respectively. The mass loss correspond to the loss of water only from the interlayer spacing of modified clays [12,13] as well as from the water of crystallisation of intercalated salt $Ni(CH_3COO)_2.4H_2O$ [14,15]. It is obvious that at this temperature the metal complex (in composite **I**) or ethylene

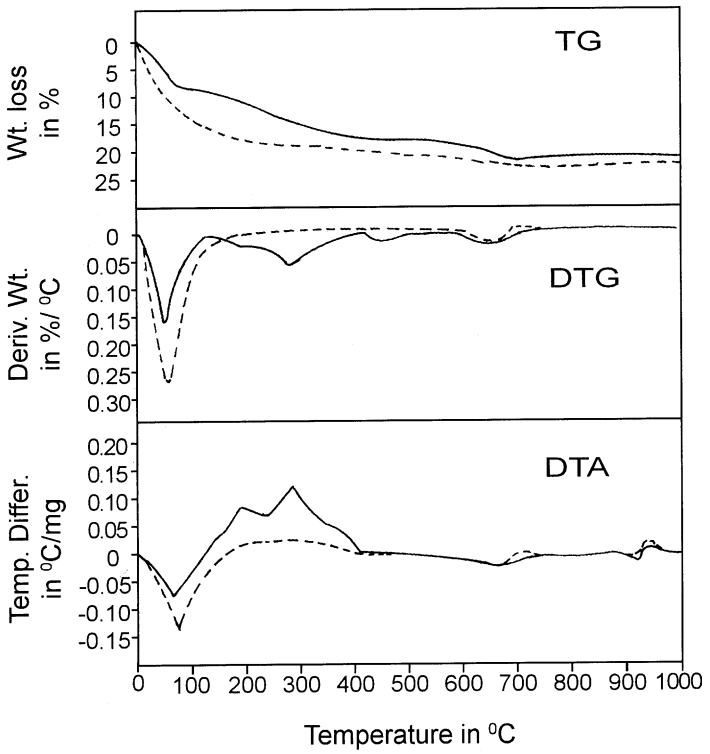

Fig. 1. The TG–DTG–DTA curves of composite **I** (dashed lines) and **II** (solid lines).

glycol if adsorbed (in composite **II**) does not decompose under air atmosphere, which is confirmed from a parallel thermal analysis conducted under nitrogen atmosphere. Moreover, at about 130 °C vaporisation of ethylene glycol is negligible due to its low vapour pressure (86.5 mm Hg). In case of Na–Mont, dehydration stage occurs within 140 °C with a mass loss of 12% as shown in Fig. 2. Each of the composites **I** and **II** shows the first endothermic DTA peaks at about 65 and 68 °C, respectively, while in case of Na–Mont, the peak occurs at about 83 °C. This difference in the peak temperatures may be associated with the higher interlayer space, i.e. basal spacings ($d_{0\,0\,1}$) of 14.2 and 14.9 Å of the intercalated composites **I** and **II**, respectively compared to that of 12.1 Å of Na–Mont.

The TG and DTG curves of composite **I** shows a mass loss of 1.8% in the temperature range 130–350 °C which is associated with formation of NiO from the decomposition of $Ni(CH_3COO)_2$ [15]. The TG and DTG curves of composite **II** show a mass loss of 7.4% in the same temperature range, i.e. 130–350 °C, which is attributable to the loss of intercalated ethylene glycol adsorbed during polyol reduction as well as its decomposition by oxidation [16]. The corresponding exothermic DTA peaks of composite **II** at 192 and 271 °C may be assigned to superimposition of exo- and endothermic peaks caused by desorption, decomposition, oxidation [16,17], etc. of ethylene glycol. From a parallel thermal analyses conducted under nitrogen, it is observed that the DTA curve of composite **II** shows only two endothermic peaks(at 225 and 295 °C) in the temperature range 130–350 °C with a mass loss (TG curve) of 5.2% attributable to loss of ethylene glycol from the clay matrix and decomposition of the organic molecules as evidenced from the blackening of the sample at this temperature range [16].

In the next stage, the TG and DTG curves of the composites **I** and **II** exhibit gradual mass loss of 4.8 and 5.3%, respectively in the temperature range 350–700 °C as compared to 4% mass loss in case of Na–Mont. In composite **I**, the mass loss is attributed to dehydroxylation caused by the breaking of structural OH-groups of Mont [12,18,19] as well as oxidation of

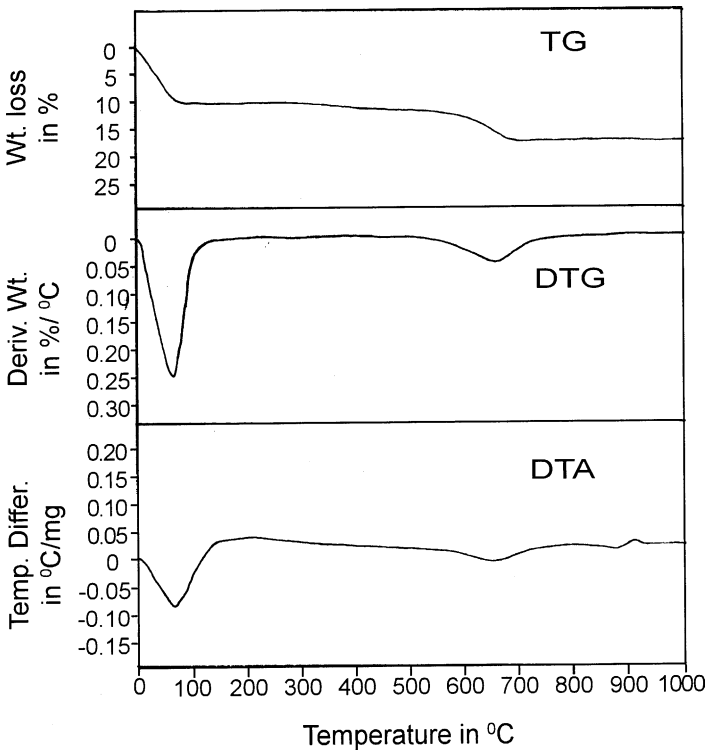

Fig. 2. The TG–DTG–DTA curves of Na–Mont.

the left out carbonaceous material from the decomposition of organic moiety [16]. While in case of composite **II**, the resultant mass loss is due to dehydroxylation [12,18,19], oxidation of the left out carbonaceous material [16] and oxidation of Ni^0 to NiO (contribute little mass gain) [5]. The DTA curves of composites **I** and **II** exhibit overall endothermic peaks at 627 and 623 °C, respectively and may be assigned to superimposition of endothermic (dehydroxylation) and exothermic (oxidation) peaks [16]. While in case of Na–Mont endothermic dehydroxylation peak occurs at 667 °C.

The composites **I** and **II** exhibit endothermic DTA peaks at 892 and 902 °C, respectively followed by exothermic peaks at around 930 °C, while Na–Mont shows the corresponding endo- and exothermic peaks at about 874 and 900 °C without any mass loss. This suggests a phase change, i.e. ordered anhydrous Mont changes to an disordered amorphous material [20,21]. Thus, it indicates that phase transformation is delayed by the presence of either $Ni(CH_3COO)_2$ or Ni^0 in the interlayers of Mont compared to Na–Mont.

The TG–DTG–DTA curves of the composites **III** and **IV** are shown in Fig. 3. The TG and DTG curves of composites **III** and **IV** show a mass loss of 14.5 and 10.7% up to 150 and 120 °C, respectively. The mass loss is attributable to dehydration of interlayer water of the modified clays [12,13]. The higher mass loss in case of composite **III** may be due to loss of water of crystallisation from the intercalated $Zn(CH_3COO)_2{\cdot}2H_2O$ [15]. The corresponding DTA curves of the composites **III** and **IV** show their respective first endothermic peaks at about 70 and 65 °C compared to 83 °C for Na–Mont. Similar to composites **I** and **II**, this shift in the peak temperature may be associated with the higher interlayer space, i.e. basal spacings ($d_{0\,0\,1}$) of 15 and 15.9 Å of the intercalated composites **III** and **IV**, respectively as compared to that of 12.1 Å of Na–Mont.

In the second stage up to 350 °C, the composites **III** and **IV** exhibit 1.8 and 8.7% mass loss, respectively and in the former the small mass loss is attributed to the decomposition of the acetate to ZnO [22]. While high mass loss in case of composite **IV** may be due to the loss of ethylene glycol molecules intercalated during polyol

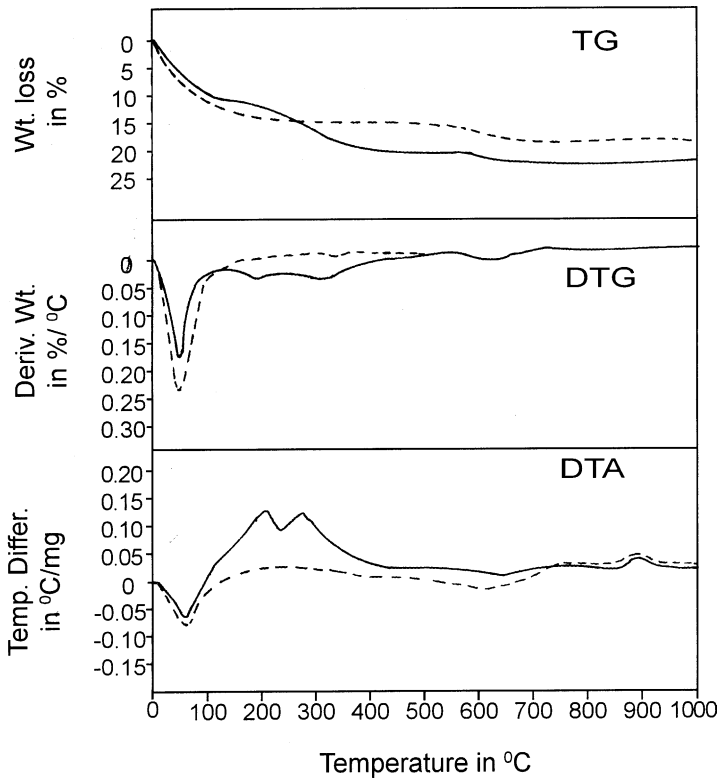

Fig. 3. The TG–DTG–DTA curves of composite **III** (dashed lines) and **IV** (solid lines).

reduction as well as its decomposition by oxidation [16]. The sharp exothermic peak in the corresponding DTA curve of composite **IV** in this temperature range may be assigned to superimposition of endo- and exothermic peaks caused by desorption, oxidation, decomposition, etc. of ethylene glycol [16,17].

The composites **III** and **IV** show a mass loss of 3.8 and 4.9 %, respectively in the temperature range 350–700 °C. In composite **III**, the mass loss is attributed to dehydroxylation caused by the breaking of structural OH-groups of Mont [12,18,19] as well as oxidation of the left out carbonaceous material from the decomposition of organic moiety [16]. The composite **IV**, on the other hand, shows a overall mass loss due to dehydroxylation, [12,18,19], oxidation of the left out carbonaceous material [16] and oxidation of Zn^0 to ZnO (contribute little mass gain) [23]. Similar to composites **I** and **II**, the DTA curves of composites **III** and **IV** exhibit overall endothermic peaks at 612 and 625 °C, respectively and may be assigned to superimposition of endothermic (dehydroxylation) and exothermic (oxidation) peaks [16].

The composite **III** shows an endothermic DTA peak at 860 °C followed by an exothermic one at 890 °C, while the composite **IV** exhibits the corresponding peaks at 850 and 880 °C with no mass loss suggesting phase transformation of Mont [20,21]. Thus, the phase change of such composites **III** and **IV** occur at lower temperature compared to those of composites **I** and **II** as well as Na–Mont.

3.2. X-ray diffraction studies

The XRD patterns along with basal spacing ($d_{0\,0\,1}$) data of the intercalated composites **I** and **II** are shown in Fig. 4. It reveals from Fig. 4a that $Ni(CH_3COO)_2.4H_2O$ molecule is intercalated into Mont because the observed basal spacing, i.e. 15.1 Å at about 50 °C is almost the summation of the thickness of the clay layer (9.6 Å) and the diameter of the nickel

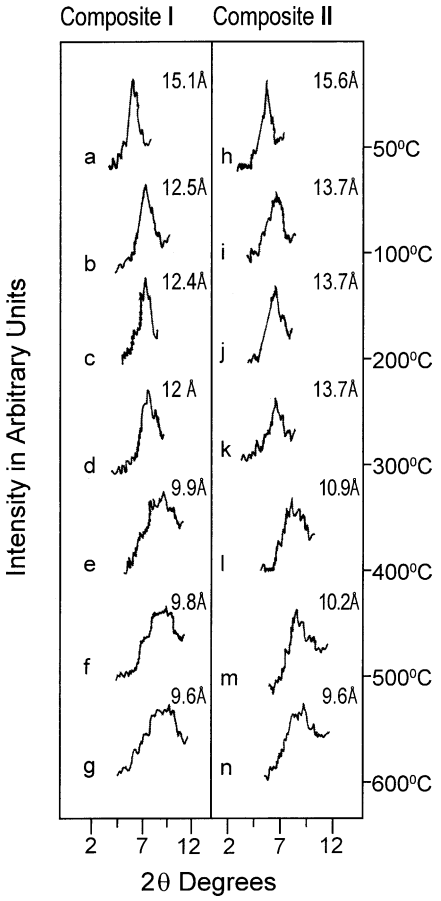

Fig. 4. The XRD patterns and basal spacing ($d_{0\,0\,1}$) of oriented samples of intercalated composite **I** (a–g) and **II** (h–n) heated at different temperatures (50–600 °C) for 1 h in air.

acetate molecule (~5.7 Å) along its trans acetate groups [24,25]. The decrease of basal spacing ($d_{0\,0\,1}$) to 12.5 Å (Fig. 4b) during heating at about 100 °C is attributed to loss of water molecules from the interlayer spacing [12,13] as well as from the water of crystallisation of nickel acetate tetrahydrate [15] substantiated by TGA data (Fig. 1). On increasing the temperature up to 200 °C, the basal spacing ($d_{0\,0\,1}$) of about 12.4 Å (Fig. 4c) is observed, which in turn decreases slightly to 12.0 Å (Fig. 4d) upon increasing the temperature up to about 300 °C indicating decomposition of the interlamellar nickel acetate to nickel oxide [15]. On further heating to 400 °C, the interlayer spacing has almost been collapsed showing a basal spacing ($d_{0\,0\,1}$) of about 9.9 Å (Fig. 4e) with multiple XRD peaks [26]. Beyond 400 °C, basal spacing ($d_{0\,0\,1}$) further lowers (Fig. 4f) and a value of about 9.6 Å is obtained at a temperature of around 600 °C (Fig. 4g) indicating complete collapse of interlayer spacing with multiple XRD peaks.

The composite **II** shows a basal spacing ($d_{0\,0\,1}$) of about 15.6 Å (Fig. 4h) at 50 °C indicating intercalation of ethylene glycol molecules [4] along with Ni^0. On heating the composite **II** up to about 100 °C for 1 h the basal spacing ($d_{0\,0\,1}$) decreases to 13.7 Å (Fig. 4i), which is attributable to loss of interlamellar water and partial expulsion of ethylene glycol from interlayers [27]. On further heating up to about 300 °C, the basal spacing ($d_{0\,0\,1}$) is found to maintain almost the same value, i.e. about 13.7 Å (Fig. 4k). This clearly indicates that Ni^0 occupy the interlayer spacing of the clay as metal clusters having a diameter of about 4.1 Å [4]. Such Ni^0 metal cluster–Mont composite heated at 400 °C exhibit $d_{0\,0\,1}$ spacing of 10.9 Å (Fig. 4l) indicating partial oxidation of the intercalated Ni^0 to NiO [5] substantiated by TGA data (Fig. 1). The basal spacing ($d_{0\,0\,1}$) further decreases to 9.6 Å at 600 °C (Fig. 4n) showing complete oxidation of nickel (Ni^0) metal to NiO and subsequent expulsion from the interlayer spacing [5] substantiated by TGA data (Fig. 1). Therefore, the in situ generated Ni^0 metal clusters are thermally stable up to about 300 °C.

The XRD patterns and basal spacing ($d_{0\,0\,1}$) data at different temperatures for composites **III** and **IV** are shown in Fig. 5. Similar to composite **I**, $Zn(CH_3COO)_2.2H_2O$ molecules, having a diameter of about 5 Å along the trans acetate groups [28], are intercalated into Mont to give a basal spacing ($d_{0\,0\,1}$) of about 15 Å (Fig. 5a) at 50 °C. Up to about 100 °C (Fig. 5b), the same basal spacing is maintained and thereafter it decreases to about 13.9 Å (Fig. 5c) at around 200 °C, which is due to loss of water molecule from the interlayer spacing as well as the water of crystallisation of the $Zn(CH_3COO)_2.2H_2O$ [15] substantiated by TGA data (Fig. 3). Further decrease of basal spacing ($d_{0\,0\,1}$) to 12.3 Å at about 300 °C (Fig. 5d) may be attributed to the decomposition of anhydrous acetate to ZnO [22]. At about 400 °C, the basal spacing ($d_{0\,0\,1}$) value becomes 10.3 Å (Fig 5e) with multiple XRD peaks which indicate almost collapse of interlayer spacing.

The composite **IV** shows a basal spacing ($d_{0\,0\,1}$) of about 16.4 Å (Fig. 5f) at 50 °C indicating intercalation

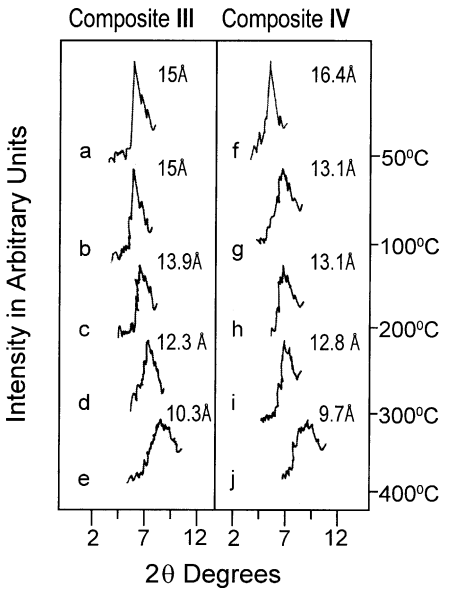

Fig. 5. The XRD patterns and basal spacing ($d_{0\,0\,1}$) of oriented samples of intercalated composite **III** (a–e) and **IV** (f–j) heated at different temperatures (50–400 °C) for 1 h in air.

of ethylene glycol molecules along with Zn^0. Such composite starts releasing the interlamellar water and ethylene glycol [27] on heating at about 100 °C as indicated by its basal spacing ($d_{0\,0\,1}$) value of 13.1 Å (Fig. 5g). Almost the same value of basal spacing ($d_{0\,0\,1}$) is maintained up to 200 °C (Fig. 5h) and then decreases slightly to 12.8 Å (Fig. 5i), while heated to about 300 °C. This reveals the presence of Zn^0 in the interlayer spacing of the clay as metal clusters having a dimension of about 3.2 Å. But basal spacing ($d_{0\,0\,1}$) decreases to 9.7 Å (Fig. 5j) at about 400 °C implying collapse of the intercalated metal clusters due to complete oxidation of Zn^0 metal to ZnO [23] substantiated by TGA data (Fig. 3), and its subsequent expulsion from the interlayers. Thus, the in situ generated Zn^0 metal clusters are stable in the interlamellar spacing of Mont up to about 300 °C.

3.3. TEM study

Most of the nanoparticles of metals grown are of round shape. It reveals that the particles grown for composite **II** are in the range of about 0–80 nm which are comparatively bigger in size than that of the composite **IV** where the particle size ranges from about 0–30 nm. Thus, it appears that most of the metal nanoparticles are not present in the interlamellar spacing of Mont as the XRD data (Figs. 4 and 5) show that the maximum size of the intercalated metal clusters is about 0.41 nm. Therefore, the bigger size nanoparticles (>0.41 nm) generated by polyol reduction process must be deposited on the external surface. The smaller metal clusters (<0.41 nm) formed in the interlamellar spacing of the clay can also agglomerate and grow in size when the clay matrix gets destroyed under the influence of electron beam (accelerating voltage is 100 kV) during the TEM experiments [3–5].

4. Conclusions

Intercalated composites **I–IV** have been synthesised and characterised by thermal analyses, XRD and TEM. The dehydration and dehydroxylation of the composites **I–IV**, in general, occur at lower temperature compared to those of untreated Na–Mont. Compared to Na–Mont, the phase change of the clay matrix for the composites **I** and **II** takes place at slightly higher temperature while that occurs at lower temperature for the composites **III** and **IV**. The XRD data show that the intercalated metal clusters in the composites **II** and **IV** are of 4.1 and 3.2 Å size, respectively and are stable up to about 300 °C. TEM study shows that the particle size of the metal cluster in the interlamellar spacing as well as on the surface of the clay layers of the composites **II** and **IV** are in the range of about 0–80 and 0–30 nm, respectively.

Acknowledgements

The authors are thankful to the Director, Regional Research Laboratory (CSIR) Jorhat, India, for his kind permission to publish the work. The authors thank Dr. P.C. Borthakur, Head, Material Science Division, RRL Jorhat, for his keen interest and support. Thanks are also due to Dr. R.L. Goswamee and Dr. R.K. Baruah, Scientists, RRL for thermal and XRD analyses. One of the authors (OSA) is grateful to University Grants Commission, New Delhi for providing a Teacher Fellowship and also to Chemistry Department, Dibrugarh University for extending the experimental facility.

References

[1] K.I. Zamaraev, V.L. Kuznetsov, in: C.N.R. Rao (Ed.), Chemistry of Advanced Materials, Blackwell Scientific Publications, Oxford, 1993 (Chapter 15).

[2] F. Fievet, J.P. Lagier, B. Blin, B. Beaudoin, M. Figlarz, Solid State Ionics 32/33 (1989) 198.

[3] P.B. Malla, P. Ravindranathan, S. Komarneni, R. Roy, Nature 351 (1991) 555.

[4] S. Ayyappan, G.N. Subbanna, R. Srinivasa Gopalan, C.N.R. Rao, Solid State Ionics 84 (1996) 271.

[5] S. Komarneni, Ceram. Trans. (Porous Mater.) 31 (1993) 155.

[6] Z. Kiraly, I. Dekany, A. Mastalir, M. Bartok, J. Catal. 16 (1996) 401.

[7] A. Mastalir, F. Notheisz, Z. Kiraly, M. Bartok, I. Dekany, in: H.U. Blaser, A. Baiker, R. Prins (Eds.), Heterogeneous Catalysis and Fine Chemicals IV, Elsevier, Amsterdam, 1997, p. 477.

[8] I. Dekany, L. Turi, Z. Kiraly, Appl. Clay Sci. 15 (1999) 221.

[9] J.E. Gillott, Clay in Engineering Geology, Elsevier, 1st Edition, 1968 (Chapter 11).

[10] A.B. Searle, R.W. Grimshaw, The Chemistry and Physics of Clays and Other Ceramic Materials, 3rd Edition, Earnest Benn, London, 1960 (Chapter 5).

[11] G.W. Brindley, G. Brown, Crystal Structure of Clay Minerals and their X-Ray Identification, Mineralogical Society, Monograph no. 5, London, 1984 (Chapter 5).

[12] R.E. Grim, Clay Mineralogy, McGraw-Hill, New York, 1953 (Chapter 9).

[13] V.C. Farmer, in: V.C. Farmer (Ed.), The Layered Silicates: The Infrared Spectra of Minerals, Mineralogical Society, Monograph no. 4, 1974, p. 331.

[14] D. Dollimore, J. Pearce, J. Therm. Anal. 6 (1974) 321.

[15] C. Balarew, D. Stoilova, J. Therm. Anal. 7 (1975) 561.

[16] S. Yariv, in: W. Smykatz-Kloss, S.St.J. Warne (Eds.), Thermal Analysis in the Geosciences, Springer, Berlin, 1991 (Chapter 38).

[17] R.C. Mackenzie, The Differential Thermal Investigation of Clays, Mineralogical Society, London, 1966, p. 160 (Chapter 5).

[18] D.N. Todor, Thermal Analysis of Minerals, Abacus Press, Tunbridge Wells, UK, 1976, p. 221 (Chapter 5).

[19] R.H. Loeppert Jr., M.M. Mortland, Clays and Clay Minerals 27 (1979) 373.

[20] R.C. Mackenzie, The Differential Thermal Investigation of Clays, Mineralogical Society, London, 1966, p. 152 (Chapter 5).

[21] D.N. Todor, Thermal Analysis of Minerals, Abacus Press, Tunbridge Wells, 1976, p. 224 (Chapter 5).

[22] B.L. Yu, Thermochim. Acta 148 (1989) 395.

[23] J.W. Mellor, A Comprehensive Treatise on Inorganic and Theoretical Chemistry, Vol. IV, Longmans & Green, London, 1957 (Chapter 30).

[24] T.C. Downie, W. Harrison, E.S. Raper, M.A. Hepworth, Acta Cryst. B27 (1971) 706.

[25] J.N. van Niekerk, F.R.L. Schoening, Acta Cryst. 6 (1953) 609.

[26] M. Bora, J.N. Ganguli, D.K. Dutta, Thermochim. Acta. 346 (2000) 169.

[27] G.W. Brindley, G. Brown, Crystal Structure of Clay Minerals and Their X-Ray Identification, Mineralogical Society, Monograph no. 5, London, 1984 (Chapter 3).

[28] J.N. van Niekerk, F.R.L. Schoening, J.H. Talbat, Acta Cryst. 6 (1953) 720.